



Cooling rate as a process parameter in advanced roll forming to tailor microstructure, mechanical and corrosion properties of EN AW 7075 tubes

Abkühlgeschwindigkeit als Prozessparameter beim fortgeschrittenen Walzprofilieren zur Anpassung von Gefüge, mechanischen und Korrosionseigenschaften von EN AW 7075-Rohren

S.V. Sajadifar¹ , T. Suckow², B. Heider³ , M. Oechsner³, P. Groche², T. Niendorf¹

The effects of solution heat treatment parameters and quench media as a processing tool for tailoring microstructure, mechanical and corrosion properties in roll forming of EN AW 7075 alloy were studied. The highest yield stress and ultimate tensile strength were obtained for the specimens quenched in water, while the air-cooled specimens exhibited inferior mechanical properties. Microstructural analysis of specimens showed that except water-quenched specimens, the parts cooled/quenched in oil, in direct contact with tool steel and air are characterized by coarse precipitates and precipitate-free zones. The corrosion tests showed that the cooling rate has a pronounced influence on the corrosion resistance and related mechanism of EN AW 7075 alloy. The surfaces of specimens quenched in water remained intact although pitting corrosion took place. The microstructure of the part processed by roll forming was explored in direct comparison. It is revealed that by the employment of quenching nozzles, a high cooling rate similar to the water-quenched condition can be achieved. Results obtained in the present study pave the way to directly tailor aluminum parts for specific applications.

Keywords: High-strength aluminum alloys / corrosion behavior / heat treatment / microstructure / fracture

Schlüsselwörter: Hochfeste Aluminiumlegierungen / Korrosionsverhalten / Wärmebehandlung / Gefüge / Bruch

¹ University of Kassel, Institute of Materials Engineering, Kassel, Germany

² Institute for Production Engineering and Forming Machines, Technische Universität Darmstadt, Darmstadt, Germany

³ Center for Structural Materials MPA-IfW, Technische Universität Darmstadt, Darmstadt, Germany

Corresponding author: S.V. Sajadifar, University of Kassel, Institute of Materials Engineering, Mönchebergstraße 3, 34125, Kassel, Germany, E-Mail: sajjadifar@uni-kassel.de

1 Introduction

Due to the extraordinary mechanical properties and the high strength-to-weight ratio of aluminum alloys, these alloys are an excellent candidate for various applications such as aerospace industries and the automotive sector [1, 2]. The T6 heat treatment, i.e. solution heat treatment followed by water quenching and subsequent artificial aging, can considerably enhance the strength of EN AW 7075 alloy [3]. Generally, the ultimate tensile strength of EN AW 7075 alloy in T6 condition was reported to be above 500 MPa, which is the highest value among the commercially available high-strength aluminum alloys [4–7]. In addition to the high ultimate tensile strength of this alloy, its acceptable formability in temperature-supported forming processes makes it a promising alternative for numerous engineering demands [8]. Recently, attempts were made to enhance the strength of EN AW 7075 in order to candidate this alloy as an alternative for steels. These attempts were mostly focused on particle hardening allowing to manufacture components with high yield strength, ultimate tensile strength and acceptable ductility [9]. One of the crucial parameters affecting the final mechanical properties of this alloy is the cooling rate from solution heat treatment temperature [10]. Water quenching of EN AW 7075 alloy leads to the formation of a supersaturated solid solution, while lower cooling rates from solution heat treatment result in the reduction in the degree of supersaturation due to the nucleation and growth of coarse η precipitates [11, 12]. Hence, the sensitivity of this alloy to the cooling rate from solution heat treatment is a great potential for the achievement of functionally graded properties in a part via the employment of various cooling rates in different areas of the component.

Many studies are also focused on the improvement of mechanical properties via grain refinement [13–17]. Severe plastic deformation techniques such as friction stir welding and friction stir processing were employed to reduce the grain size in metallic materials. By optimization of hot rolling and friction stir processing parameters, the superplastic behavior of materials was achieved [13, 18]. Equal-channel angular pressing was also utilized to improve the mechanical properties of additively manufactured aluminum alloy [19]. It was found

that equal-channel angular pressing is capable of enhancing the mechanical properties of AlSi12 alloy with minimum coarsening of fine silicon network formed upon laser-based powder bed fusion.

Not only poor mechanical properties of metallic materials but also their low corrosion resistances can limit their utilization in engineering applications. Thus, efforts were made to reveal the effect of morphology, size and distribution of second-phase particles, i.e. precipitates, in the EN AW 7075 alloy [20, 21]. It was reported that the susceptibility to localized corrosion of EN AW 7075 alloy in the T6 condition adversely affects the qualities of the final parts although this alloy in the T6 state exhibits excellent mechanical properties [22]. The potential difference between matrix and second-phase particles is a driving force for the occurrence of the corrosion [23]. To avoid an adverse influence of precipitates the corrosion resistance of EN AW 7075 alloy, T73 state, also referred to as over-aged, can be used. The content of copper in the introduced precipitates is a key parameter for the corrosion resistance of this alloy [24]. Introduced second-phase particles in the T73 condition contain a higher amount of copper leading to lower anodic and cathodic reaction rates and, eventually, lower corrosion rates [25]. However, T73 heat treatment causes nearly 15 % reduction in the ultimate tensile strength of this alloy compared to that of the T6 condition [24]. Therefore, simultaneous improvement in mechanical behavior and corrosion resistance of EN AW 7075 alloy is one of the major challenges for manufacturers and industrial sectors for substituting steels with high-strength aluminum alloys.

Towards the industrialization of high-strength aluminum alloys, one of the key challenges is to manufacture a product meeting all requirements in terms of mechanical properties, corrosion resistance and cost-effectiveness. Owing to the incremental character of roll forming, this process proved to be suitable to realize long profiles with high production efficiency and formability [26]. As starting condition for the 7075 alloy, the T6-condition (solution heat-treated and artificially aged) is used for the roll forming process, *Figure 1*. After roll forming, a welding operation follows to close the tube. During the subsequent heat treatment, the tube is heated up by induction to the solution annealing temperature of 480 °C and quenched afterwards.

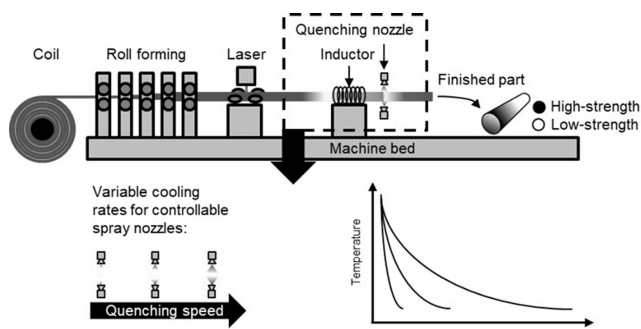


Figure 1. Process chain for the production of high-strength EN AW 7075 tubes. Schematics of controllable spray nozzle and temperature versus time plot displaying cooling rate are shown in the bottom row of figure.

For control of the quenching speed on the tube, quenching is carried out with controllable spray nozzles. Due to the high quench sensitivity of the EN AW 7075 alloy, the tube finally features areas with varying degrees of supersaturation resulting in tailored mechanical properties in the subsequent aging treatment after welding [5, 27]. Thus, after implementation of apt process parameters this approach can significantly improve the process chain for producing graded EN AW 7075 tubes.

To optimize process parameters and understand the impact of different cooling rates during quenching in the roll forming process on the microstructure evolution, corrosion behavior and mechanical properties of EN AW 7075, various quenching media, i.e. water, oil, direct contact to a steel tool and air, were used in the present study. Here, the application of different quenching media is the basis to establish the interrelationships between well-known microstructures induced by quenching and the variable quenching efficiency by adjustable spray nozzles. Furthermore, the microstructure of the part roll-formed, quenched via a spray nozzle and subsequently aged is studied in depth to better understand the process—microstructure—corrosion-property relationships. Previous studies on high-strength aluminum alloys have

shown that different cooling rates implemented via heated tools can be used to tailor microstructure and properties [5, 6, 28, 29]. In analyzing the present state-of-the-art, it is clear that there is a lack of data exploring the effects of different quenching media on corrosion behavior, microstructural evolution and mechanical properties. Therefore, the heat treatments in the experiments were conducted similar to the industrial application of heat treatments in the roll forming processes. From these experiments, conclusions are drawn with respect to the solution heat treatment temperature and quenching media to eventually deduce optimized process parameters for realizing targeted microstructure at the given spot.

2 Materials and experimental details

2.1 Materials and heat treatment experiments

EN AW 7075 in T6 condition with a thickness of 1.5 mm were received in sheet form. The sheets of the coiled material were supplied by AMAG Company (Ranshofen, Austria). According to the standard EN 573-3, the optical emission spectroscopy technique was used for determination of chemical composition, *Table 1*.

With the aim of tailoring mechanical properties, different solution heat treatment temperatures (460 °C to 500 °C), various soaking times (1 min to 60 min) and different quench media (water, oil, air and direct contact with a steel plate at room temperature) were employed to study the influence of solution heat treatment parameters on the mechanical properties, microstructural evolution and corrosion behavior of EN AW 7075 alloy. All specimens were subsequently aged at 120 °C for 24 hours. A Nabertherm N41/H furnace was used to conduct solution and aging heat treatments. Thermocouples were attached to holes in the sheets with a diameter of 1 mm to measure the exact temperature of the

Table 1. Chemical composition of the EN AW 7075 alloy used in the present study.

Element	S	Fe	Cu	Mn	Mg	Cr	Zn	Ti	Zr	Al
AA7075 (Wt.-%)	0.10	0.11	1.49	0.03	2.38	0.20	5.57	0.03	0.04	Balance

specimens during heat treatments in accompanying experiments.

2.2 Tensile experiments

Tensile specimens were cut from the sheet by milling with gage section dimensions of 75 mm × 12.5 mm × 1.5 mm (according to DIN 50125). Ambient temperature tensile tests were conducted at a nominal crosshead speed of 0.2 mm/s by Zwick Roell 100 tensile testing machine equipped with a 100 kN load cell. Three experiments were carried out for each condition and the average values of yield strength, ultimate tensile strength and elongation at fracture are reported. During tensile tests, elongation values were measured using a Zwick videoXtens video extensometer.

2.3 Microstructural analysis

Microstructural evolution was analyzed utilizing a scanning electron microscope. Both back-scattered electron and secondary electron modes were used to study the microstructure and fracture morphology of the alloy in different conditions. Back-scattered electron and secondary electron modes were employed at the accelerating voltages of 30 kV and 20 kV, respectively. For microstructural studies, specimens were first ground to 5 μm grit size and polished using a colloidal silica suspension.

2.4 Corrosion testing

Corrosion testing was performed according to the standard DIN EN ISO 11846 procedure B, i.e. testing for the susceptibility for intercrystalline corrosion of precipitation-hardenable aluminum alloys. The procedure consists of etching in 5 % sodium hydroxide solution at 50 °C–60 °C for 2.5 min, rinsing with water, then neutralizing in concentrated nitric acid for 2 min, rinsing and air drying. The corrosion tests were done by immersing the specimens in a solution of 3 % sodium chloride with 1 % hydrogen chloride for 24 h at room temperature. After the tests, the specimens were rinsed with water and corrosion products were removed by immersing in concentrated nitric acid. After the

tests, the surface appearance was documented using a digital microscope Keyence VHX-6000 and cross-sections were prepared for metallographic investigations.

3 Results and discussion

3.1 Mechanical properties

The effect of solution heat treatment temperature on the mechanical properties of EN AW 7075 alloy is explained in this section. All specimens were solutionized for 5 min followed by water quenching and aging at 120 °C for 24 h. With the increase in solution heat treatment temperature from 460 °C to 500 °C, a slight increase in yield strength and ultimate tensile strength values was observed, *Figure 2a*. It is well known that a higher solution heat treatment temperature results in the complete dissolution of precipitates in as-received condition due to the higher diffusion rate of alloying elements at relatively high temperatures. As a result of the complete dissolution of particles, the degree of supersaturation increases leading to a more efficient precipitation process in the subsequent aging treatment [30]. The influence of soaking time on the mechanical properties of this alloy is considered. Solution heat treatments of these specimens were performed at 480 °C, which is the recommended solution heat treatment temperature for EN AW 7075 alloy [5, 30]. Then, specimens were water-quenched and aged at 120 °C for 24 h. Even 1 min of soaking at 480 °C might be sufficient to dissolve the second-phase particles, *Figure 2b*. The impact of the soaking time on the mechanical properties is somehow complex since several phenomena, e.g. dissolution of precipitates and grain growth affecting the strength of the alloy, can be effective simultaneously [31, 32]. Thus, more detailed studies are required to assess the effect of soaking time on the microstructure in more detail. Tensile properties and cooling rates of specimens quenched using different media are reported herein. All specimens were solution heat treated at a temperature of 480 °C for 5 min and aged at 120 °C for 24 h. The highest yield strength and ultimate tensile strength values were achieved for the specimens quenched in water and oil, while the air-cooled specimen showed poor mechanical properties, *Figure 2c*. Ela-

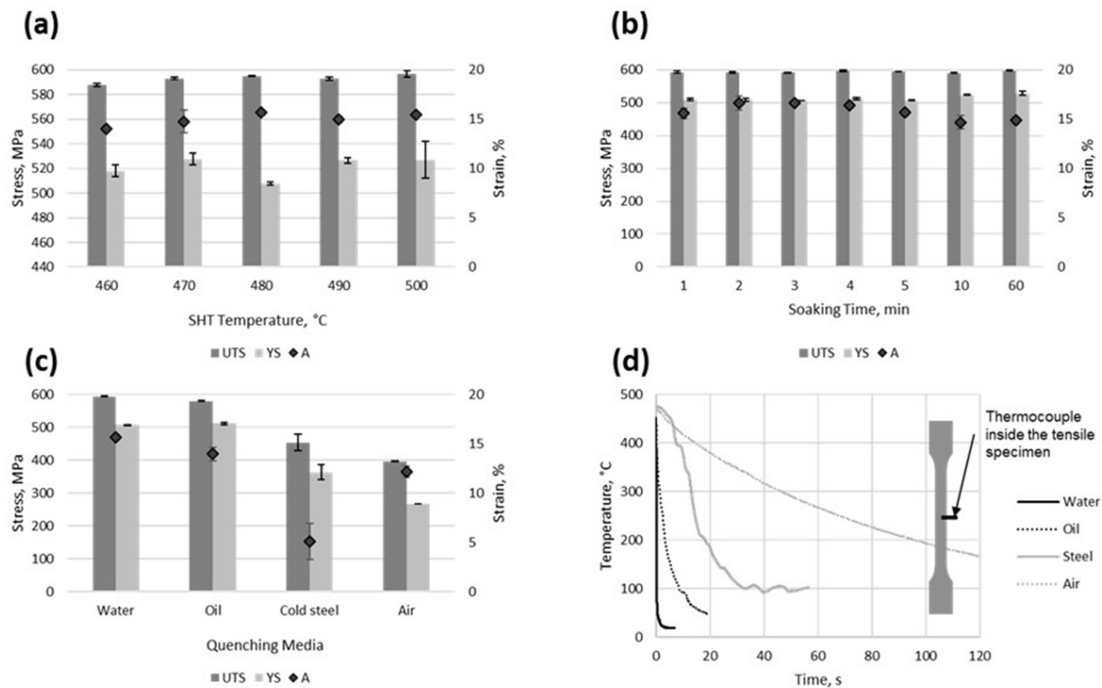


Figure 2. (a) Influence of different solution heat treatment temperatures at a soaking time of 5 min followed by water quenching and aging at 120 °C for 24 h, (b) effect of soaking times at a solution heat treatment temperature of 480 °C followed by water quenching and aging at 120 °C for 24 h and (c) effect of different quench media for specimens solution heat treated at a temperature of 480 °C and a soaking time of 5 min on the tensile properties of EN AW 7075 alloy; (d) Temperature versus time plot for specimens quenched in accompanying experiments using different quenching media.

borated mechanical properties can be rationalized by the cooling rate after solution heat treatment, Figure 2d. Due to the high cooling rates for the specimens quenched in water, the formation of coarse precipitates during cooling is prevented eventually leading to a high degree of supersaturation. The higher degree of supersaturation in those conditions led to the formation of fine and well-dispersed second-phase particles in the subsequent artificial aging treatment. It is well-established that interparticle spacing is low for specimens containing fine precipitates [33, 34]. This intensifies dislocation-precipitate interactions and eventually results in the strengthening of the material.

3.2 Microstructural evolution

Based on the mechanical properties detailed in the previous subchapter, conditions were selectively chosen for microstructural studies. Back-scattered electron images of specimens quenched from solution heat treatment in various media were taken.

Evidently, no coarse precipitates were observed in the specimens quenched in water, Figure 3a. However, the sheets quenched in oil, in direct contact to tool steel and air contain coarse precipitates formed in direct vicinity of grain boundaries, Figure 3b–d. Previous studies showed that these coarse precipitates are close to the stoichiometric compositions of the eta phase [10, 35, 36]. Due to the growth of coarse grain boundary precipitates, the alloying elements required for precipitation are already absorbed and eventually only a minimized fraction of fine precipitates (eta prime) evolves within the following aging treatment. Thus, the fraction of fine precipitates being present in these conditions does not provide for efficient strengthening of the alloy [10, 37, 38]. Besides, the reduction of alloying elements in the surrounding zones of the coarse grain boundary precipitates promotes the evolution of a precipitate-free zone [35, 39–42]. It was previously reported that the formation of precipitate-free zones is very detrimental to the mechanical properties of aluminum alloys [39, 43]. A direct comparison of the size of precipitates in different specimens quenched in various media reveals that the speci-

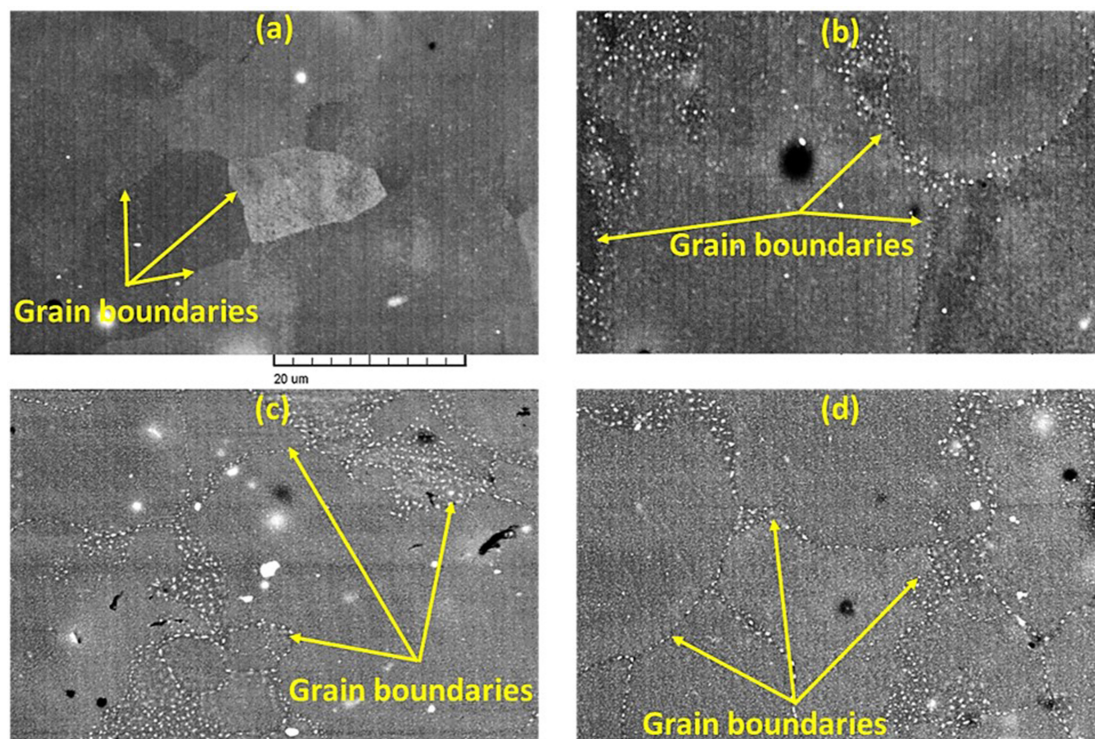


Figure 3. Back-scattered electron images detailing microstructure evolution for the specimen quenched in (a) water, (b) oil, (c) direct contact to tool steel and (d) air; all specimens were solution heat treated a temperature of 480 °C and a soaking time of 5 min followed by aging treatment. Selected grain boundaries are marked by yellow arrows.

mens cooled in the air contain the coarsest precipitates. The specimens quenched in water were expected to be characterized by the finest precipitates. However, the fine precipitates in the water-quenched specimens could not be resolved via the back-scattered electron technique and, thus, further studies via high-resolution transmission electron microscopy are needed. However, such an analysis is beyond the scope of the current study and, thus, will be the subject of follow-up work.

Back-scattered electron micrographs of specimens solution heat treated for a soaking time of 5 min followed by water quenching and subsequent artificial aging confirmed that solution heat treatment at a temperature of 460 °C cannot lead to the complete dissolution of precipitates as partially dissolved precipitates are evident on the micrograph of this condition, *Figure 4*. Fine precipitates presented in the T6 condition were coarsened in the heating cycle from room temperature to solution heat treatment temperature. Coarsened precipitates were completely dissolved during exposure at a high solution heat treatment temperature of 500 °C, however, these particles were only partially dissolved at

a low solution heat treatment temperature, e.g. at 460 °C, due to the insufficiency of thermal energy provided [44].

3.3 Corrosion behavior

Obviously, the influences of the quenching rate, solution heat treatment temperature and dwell time on the corrosion appearance are strong even after artificial aging, *Figure 5*. Susceptibility to intercrystalline corrosion was investigated following DIN EN ISO 11846. The surface of the specimen quenched in water is still intact despite localized attacks observed, however, the surfaces of the specimens quenched in direct contact to the tool steel and air-cooled condition were completely dissolved during testing. The surface of the specimen quenched in oil is barely intact. Following water quenching, intercrystalline corrosion attacks are seen at the surface. These progressed deeper into the material. Eventually, due to oxygen deprivation in the medium that is caused by limited oxygen exchange in the corrosion paths, the pH value de-

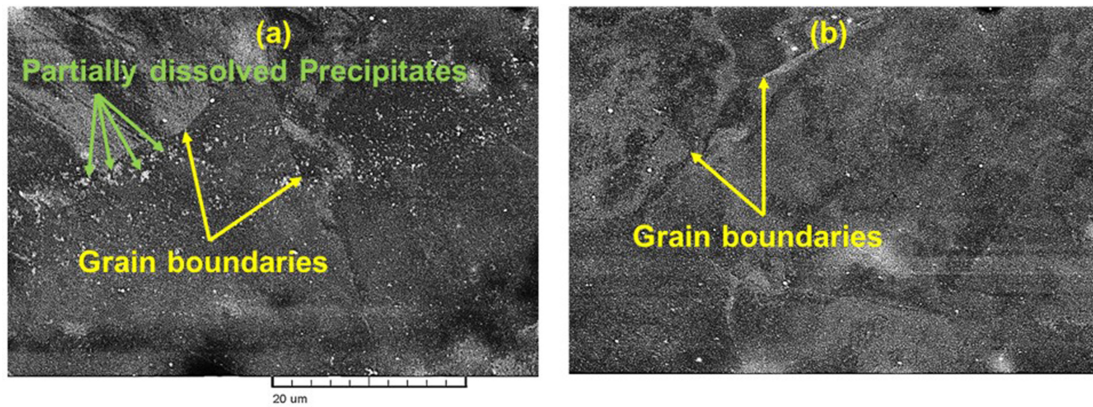


Figure 4. Back-scattered electron images detailing the microstructure of specimens solution heat treated at temperatures of (a) 460 °C and (b) 500 °C for 5 min followed by water quenching and subsequent aging at 120 °C for 24 h. Selected grain boundaries and only partially dissolved precipitates are marked by yellow and green arrows, respectively. See text for details.

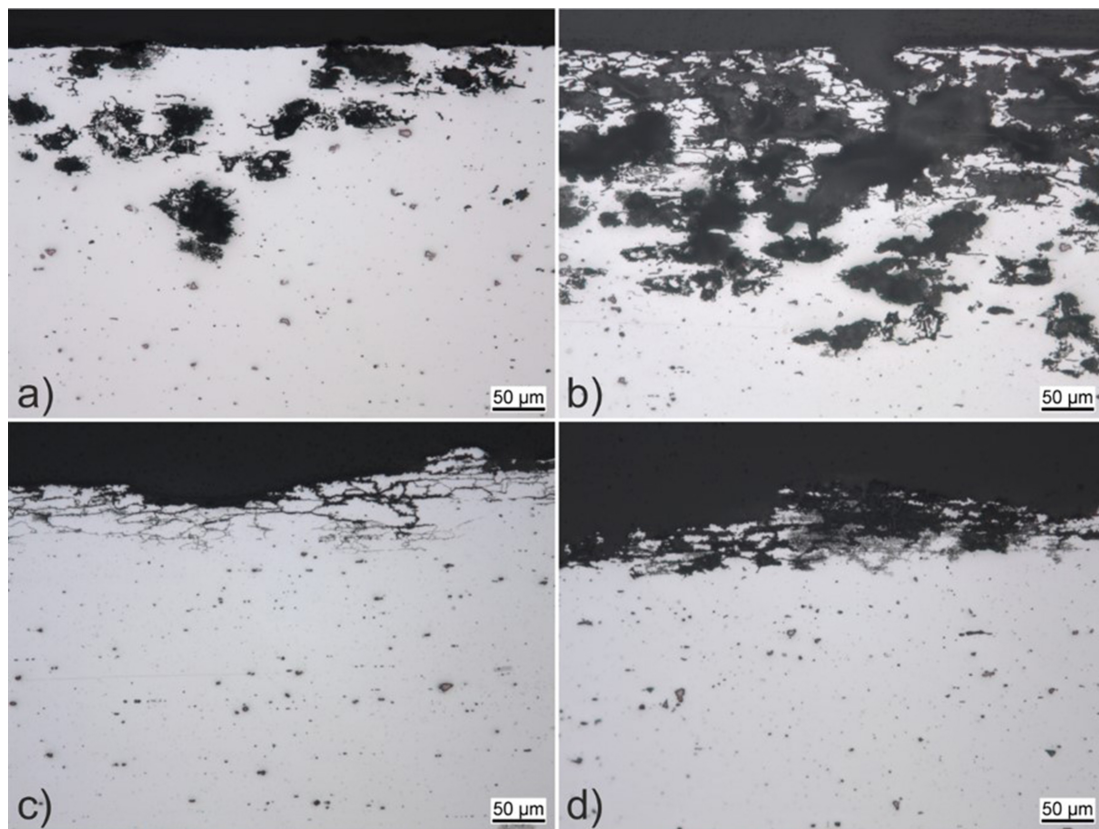


Figure 5. Micrographs of the cross-sections of the specimen quenched in (a) water, (b) oil, (c) direct contact to tool steel and (d) air after corrosion testing; all specimens were solution heat treated at a temperature of 480 °C for a soaking time of 5 min followed by aging treatment.

creases and the medium becomes more aggressive, leading to pitting corrosion underneath the surface. The corrosion mechanism after oil quenching appears to be similar in principle, but much more pro-

nounced with very densely distributed intercrystalline corrosive attacks at the surface. However, as discussed before, the lower quenching rate leads to formation of coarse precipitates, presumably eta

particles at the grain boundaries that are attacked by the corrosive medium. Those eta precipitates are anodic to the matrix and especially to the precipitate-free zones in the vicinity of the grain boundaries [21]. Therefore, the particles dissolve anodically. Due to a large number of precipitates at the grain boundaries, the corrosion is intense and possibly entire grains are separated after dissolution of the grain boundary. For the specimen quenched in direct contact with the tool steel, intercrystalline corrosion took place to such a strong degree, that the surface appears completely dissolved. The corrosion seems to follow the grain boundaries until the single grains are not bound in the microstructure and released from the sheet metal into the medium. Similarly, but with additional general corrosion attack, i.e. a plane appearance of corrosion, of the aluminum matrix, the surface of the specimen cooled in air after solution heat treatment was completely dissolved.

Obviously, the corrosion depth with respect to the specimen surface cannot be determined for the specimens quenched in contact to the tool steel or in air. For the specimens quenched in oil or water the corrosion attacks and corrosion depth were experimentally determined, *Table 2*. Although the

standard deviation is high, there is a trend towards lower numbers and lower average corrosion depth with increasing solution heat treatment duration at 480 °C, reaching a minimum average corrosion depth at 10 min solution heat treatment at 480 °C. Considering shortened process times, it can be assumed that with a solution heat treatment temperature of 480 °C, the duration could be reduced to 5 min–10 min with respect to an acceptable corrosion behavior of the aluminum alloy in focus.

Focusing on various solution heat treatment temperatures from 460 °C to 500 °C for a duration of 5 min, changes in the corrosion mechanisms become obvious, *Figure 6*. At 460 °C, the temperature seems not to be sufficient for homogenization of the alloy and dissolution of coarse precipitates formed during heating from room temperature to the solution heat treatment temperature, *Figure 4*. This leads to severe intercrystalline corrosion and complete dissolution of the surface, *Figure 6*. At 470 °C, the average corrosion depth is lower, yet there is a change towards pitting corrosion. For a solution heat treatment at 490 °C, the intercrystalline corrosion and pitting corrosion are occurring simultaneously, while for 500 °C, it is mainly pitting corrosion. The average corrosion depths de-

Table 2. Number of corrosion attacks and average depth for the differently solution heat treated, quenched and aged specimens after corrosion testing.

Specimen	Number of corrosion attacks	Average corrosion depth [μm]
1 min 480 °C, Water, T6	23	177 \pm 43
2 min 480 °C, Water, T6	26	169 \pm 30
3 min 480 °C, Water, T6	25	143 \pm 37
4 min 480 °C, Water, T6	21	155 \pm 51
5 min 480 °C, Water, T6	15	129 \pm 46
10 min 480 °C, Water, T6	23	118 \pm 44
60 min 480 °C, Water, T6	11	140 \pm 59
5 min 480 °C, Oil, T6	27	262 \pm 35
5 min 480 °C, Tool steel, T6	General corrosion	–
5 min 480 °C, Air, T6	General corrosion	–
5 min 460 °C, Water, T6	General corrosion	–
5 min 470 °C, Water, T6	34	73 \pm 30
5 min 490 °C, Water, T6	11	121 \pm 29
5 min 500 °C, Water, T6	21	72 \pm 25

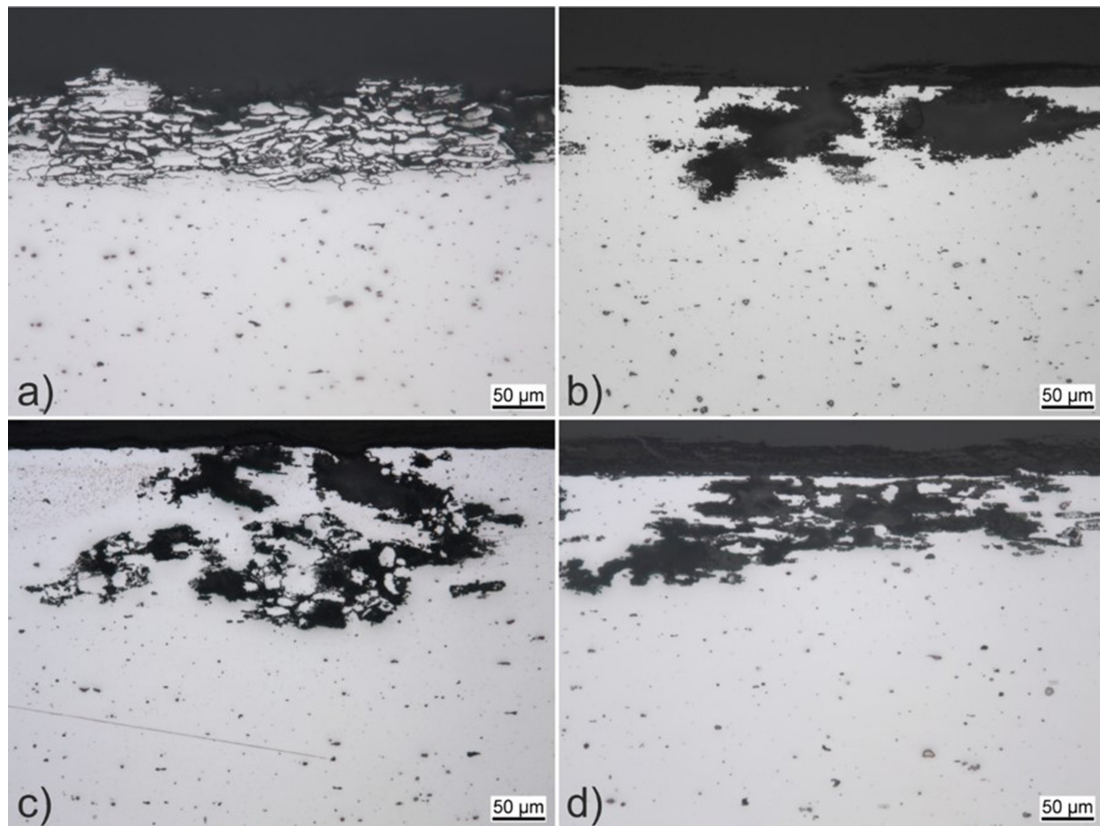


Figure 6. Micrographs of the cross-sections of the specimens solution heat treated for 5 min at (a) 460 °C, (b) 470 °C, (c) 490 °C and (d) 500 °C after corrosion testing; all specimens were water-quenched and artificially aged after solution heat treatment.

terminated for 470 °C and 500 °C are lower than for 480 °C, but the corroded volume of the pits is obviously much higher. For a solution heat treatment at 490 °C, the average corrosion depth and corrosion appearance are similar to those at 480 °C.

3.4 Fractography

The fracture surfaces upon tensile testing of specimens quenched in different media were investigated. Fracture morphology of all specimens can be classified as a ductile failure since dimple-like facets are evident on all fracture surfaces, *Figure 7*. Slip markings, traces of ductile failure, can also be observed on the fracture surfaces. Another detail present on the fracture surfaces of different specimens is the trace of the de-cohesion of coarse particles from the matrix. Weak precipitates/matrix interfaces provide suitable sites for crack initiation [45, 46]. The size of these particles is larger for the

specimens quenched in the air compared to other conditions. This can be rationalized by the low cooling rate from solution heat treatment in air-cooled specimens providing enough time for the nucleation and growth of relatively coarse precipitates.

3.5 Process-microstructure-corrosion-property relationships

To establish the process-microstructure-corrosion-property relationships, the microstructure of the part roll-formed, quenched by the nozzle spray and subsequently aged was characterized using back-scattered electron techniques. The microstructure of the processed part contains some relatively coarse precipitates along the grain boundaries, *Figure 8*. The sizes of grain boundary precipitates in the processed part are below those introduced in the specimens quenched in oil and direct contact with

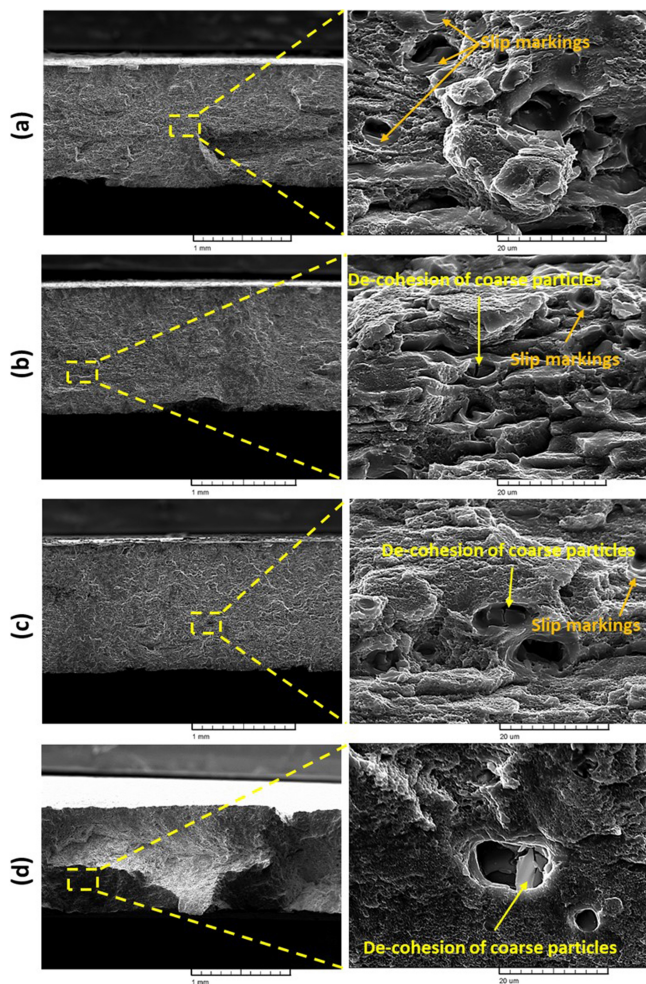


Figure 7. Fractographs upon tensile testing of specimens quenched in (a) water, (b) oil, (c) direct contact to tool steel and (d) air; scanning electron microscope images at higher magnification are shown and marked with yellow dashed rectangles. Specific features captured on the fracture surfaces are marked by arrows.

tool steel. This finding reveals that the cooling rate in the process can even reach values close to the cooling rate in water quenching. Such a high cooling rate from the solution heat treatment in the process shortened the time for the growth of the formed precipitates along the grain boundaries and, thus, a higher degree of supersaturation eventually promoting an effective aging treatment. Based on the microstructural evolution, it can be expected that the mechanical and corrosion properties of the processed parts examined here would be between water and oil-quenched specimens.

A schematic details the impact of the cooling rate to deduce the relevant solution heat treatment–mechanical property–microstructure–corrosion be-

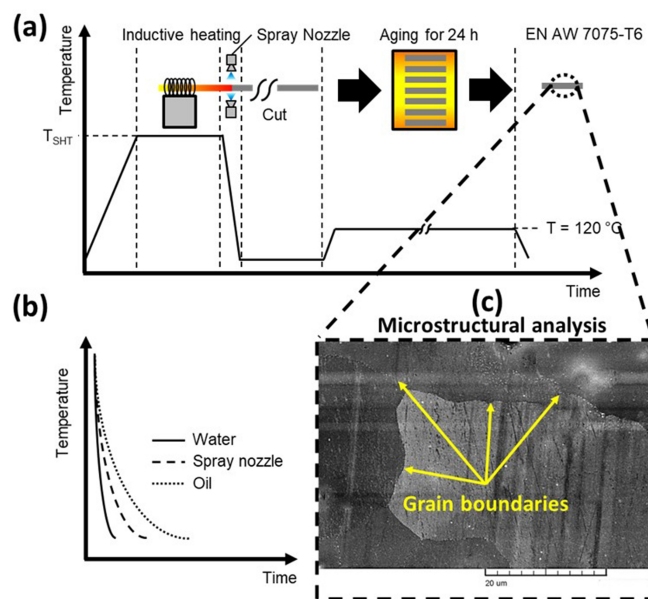


Figure 8. (a) Schematic detailing the process route containing inline solution heat treatment, quenching using spray nozzles and aging for 24 h; the region of microstructural analysis is also shown; (b) schematic highlighting the cooling efficiency of different setups; (c) back-scattered electron image of part roll-formed, quenched by the spray nozzle and aged. Selected grain boundaries are marked by arrows.

havior relationships, *Figure 9*. As discussed before, higher cooling rates result in superior mechanical properties. This can be ascribed to the morphologies and sizes of precipitates formed in the microstructure. Higher cooling rates lead to the formation of a high degree of supersaturation and, eventually, the formation of fine precipitates in the subsequent aging treatment as schematically displayed. The formation of fine and dispersed precipitates promotes low interparticle spacing. Low interparticle spacing is a key element in the strengthening of high-strength aluminum alloys since dislocation motion can be considerably impeded due to the dislocation–precipitate interactions [45, 47]. However, coarse precipitates are formed in the vicinity of grain boundaries after the employment of low cooling rates as schematically shown. The formation of these coarse precipitates results in the depletion of alloying elements in the microstructure and a reduction in the degree of supersaturation. Eventually, such evolution impedes the formation of fine precipitates in the subsequent aging treatment [10, 46, 48]. Different microstructures resulting from various cooling rates led to entirely different corrosion mechanisms. Coarse η precipitates are anodic

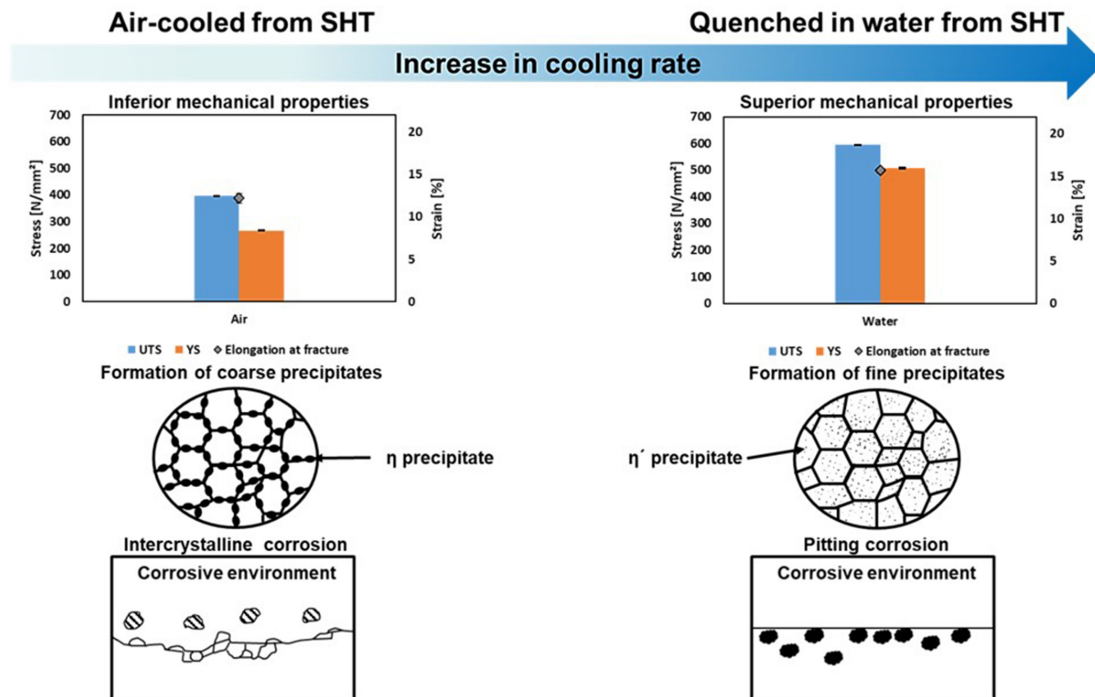


Figure 9. Schematic illustration highlighting the impact of cooling rate from solution heat treatment on microstructure evolution, mechanical properties and corrosion behavior. See text for details.

to the precipitate-free zones causing severe corrosion along the grain boundaries. Thus, coarse precipitates are responsible for the intercrystalline corrosion being seen in the specimens cooled/quenched from solution heat treatment at lower rates. Intercrystalline corrosion driven by coarse precipitates along grain boundaries was numerous reported for aluminum alloys [49, 50]. Although the surfaces of specimens cooled/quenched from solution heat treatment at high rates remain intact, pitting corrosion took place underneath the surfaces. As discussed before, a reduction in pH level is the main reason for the occurrence of pitting corrosion. Fine eta prime precipitates present in the microstructure of water and oil-quenched specimens are mostly cathodic to the matrix resulting in a potential difference and eventually pitting corrosion [51].

Finally, solution heat treatment temperature-mechanical property-microstructure-corrosion behavior relationships are schematically established, *Figure 10*. The solution heat treatment temperature slightly affects the mechanical properties of EN AW 7075 alloy. Basically, a higher solution heat treatment temperature (up to 500 °C) gradually enhances yield strength and ultimate tensile strength

values compared to those obtained after solution heat treatment at lower temperatures. As schematically highlighted, in case of a low solution heat treatment temperature, thermal energy may not be sufficient for the complete dissolution of precipitates being present in as-received condition [44]. Eventually, these partially dissolved precipitates can lower the degree of supersaturation resulting in a lower volume fraction of fine precipitates upon subsequent aging treatment. The impact of the solution heat treatment temperature on the corrosion resistance of EN AW 7075 alloy seems to be very significant although it is not very noticeable on the mechanical properties of this alloy. Lower solution heat treatment temperatures promote the occurrence of intercrystalline corrosion, however, higher solution heat treatment temperatures cause pitting corrosion. Presence of partially dissolved precipitates, presumably in the vicinity of grain boundaries, in the specimens solution heat treated at lower temperatures could be the main reason for the intercrystalline corrosion. Potential difference between these particles and surrounding areas is the driving force for corrosion [52].

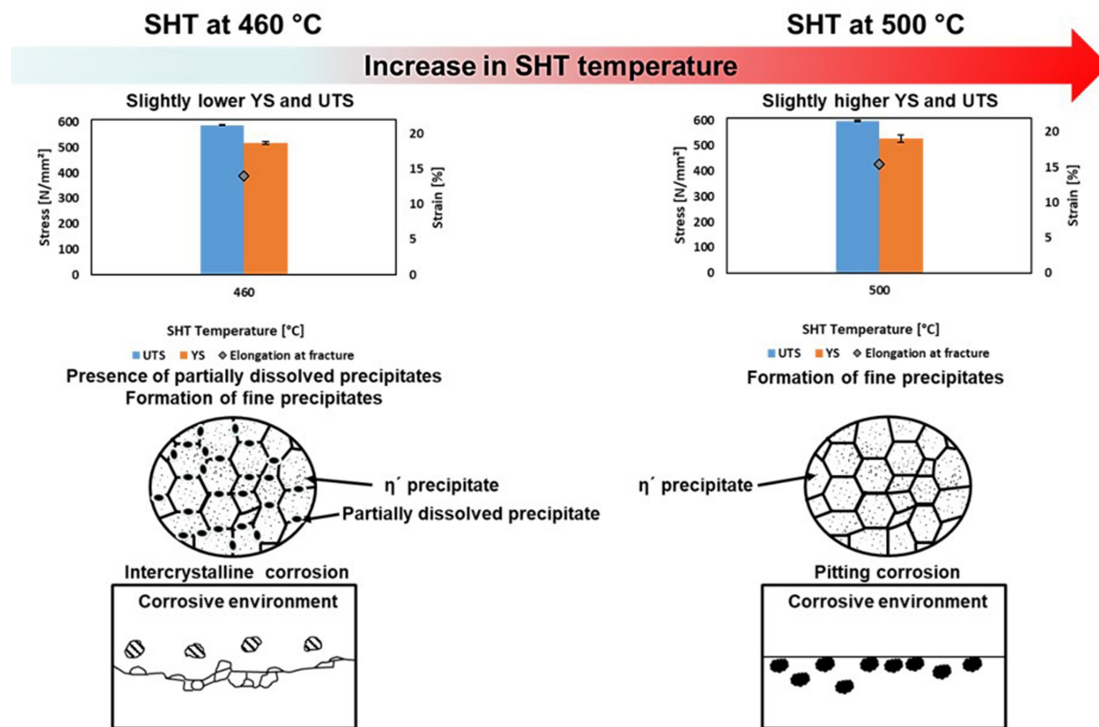


Figure 10. Schematic illustration highlighting the impact of the solution heat treatment temperatures on microstructure evolution, mechanical properties and corrosion behavior. See text for details.

4 Conclusions

In the present study, different solution heat treatment parameters and various quench media were used to explore the feasibility of tailoring microstructure, corrosion behavior and mechanical properties of EN AW 7075 alloy. The analysis of mechanical behavior, corrosion resistance and microstructural evolution showed that it is possible to obtain graded EN AW 7075 parts in advanced processes, e.g. temperature-assisted roll forming. The following conclusions can be drawn from the results presented:

1. The influence of solution heat treatment temperature and soaking time on the mechanical properties of EN AW 7075 alloy in the parameter window explored is not very pronounced. However, with the increase of solution heat treatment temperature, a gradual increase in yield strength and ultimate tensile strength is seen. On the contrary, the quench medium has a strong impact on the mechanical properties of the final parts. Specimens quenched in water exhibit the highest yield strength and ultimate tensile strength,

while the specimens cooled in air show poor mechanical properties.

2. Back-scattered electron analysis of specimens quenched in different media reveals that the very high cooling rate in water quenching can prevent the formation of coarse precipitates in the vicinity of grain boundaries. The parts quenched in oil, direct contact with tool steel and air consist of coarse grain boundary precipitates and precipitate-free zones adversely affecting the mechanical properties of EN AW 7075 alloy. Microstructural assessment of specimens solution heat treated at different temperatures revealed that at the high solution heat treatment temperature of 500 °C, dissolution of precipitates being present in as-received condition completely took place. However, the second-phase particles were only partially dissolved at the low solution heat treatment temperature of 460 °C.
3. The corrosion behavior is governed by the microstructure and precipitation kinetics during cooling and artificial aging. It is most strongly influenced by the quenching rate after solution heat treatment. Water quenching is the only

choice to avoid very intense intercrystalline and general corrosion. After solution heat treatment at 480 °C, water quenching and aging the average depth of intercrystalline corrosion is reduced, when solution heat treatment of 5 min to 10 min are considered.

4. Analysis of fracture surfaces implies that ductile failure took place in all conditions. De-cohesion of coarse particles from the matrix and slip markings are characteristic for the fracture surfaces. The particles detected on the fracture surface of the air-cooled specimen are considerably larger than those in the other conditions.
5. Microstructural analysis of the part roll-formed, quenched via spray nozzles and aged revealed that a cooling rate close to the water-quenched condition can be reached in the advanced thermo-mechanical process in focus. These findings pave the way towards robust processing of locally tailored, high-strength aluminum alloys with excellent mechanical and corrosion properties.

Acknowledgements

The authors gratefully acknowledge financial support from the Hessen State Ministry for Higher Education, Research and the Arts-Initiative for the Development of Scientific and Economic Excellence (LOEWE) for the Project ALLEGRO (Subprojects A1, B1 and B3). Open access funding enabled and organized by Projekt DEAL.

5 References

- [1] E.A. Starke, J.T. Staley, *Prog. Aerosp. Sci.* **1996**, *32*, 131. DOI: 10.1016/0376-0421(95)00004-6.
- [2] M. Tisza, I. Czinege, *Int. J. Light. Mater. Manuf.* **2018**, *1*, 229. DOI: 10.1016/J.IJLMM.2018.09.001.
- [3] K. Senthil, M.A. Iqbal, P.S. Chandel, N. Gupta, *Int. J. Impact Eng.* **2017**, *108*, 171. DOI: 10.1016/J.IJIMPENG.2017.05.002.
- [4] B. Hu, I.M. Richardson, *Mater. Sci. Eng. A.* **2007**, *459*, 94. DOI: 10.1016/j.msea.2006.12.094.
- [5] S.V. Sajadifar, E. Scharifi, U. Weidig, K. Steinhoff, T. Niendorf, *HTM J. Heat Treat. Mater.* **2020**, *75*, 177. DOI: 10.3139/105.110412.
- [6] S.V. Sajadifar, E. Scharifi, U. Weidig, K. Steinhoff, T. Niendorf, *Metals (Basel)*. **2020**, *10*, 884. DOI: 10.3390/met10070884.
- [7] S.V. Sajadifar, P. Krooß, H. Fröck, B. Milkereit, O. Kessler, T. Niendorf, *Met.* **2021**, *11*, 1142. DOI: 10.3390/MET11071142.
- [8] B.A. Behrens, S. Hübner, H. Vogt, O. Golovko, S. Behrens, F. Nürnberger, *IOP Conf. Ser. Mater. Sci. Eng.* **2020**, *967*, 012017. DOI: 10.1088/1757-899X/967/1/012017.
- [9] P. Das, R. Jayaganthan, I.V. Singh, *Mater. Des.* **2011**, *32*, 1298. DOI: 10.1016/j.matdes.2010.09.026.
- [10] S.V. Sajadifar, G. Moeini, E. Scharifi, C. Lauhoff, S. Böhm, T. Niendorf, *J. Mater. Eng. Perform.* **2019**, *28*, 5255. DOI: 10.1007/s11665-019-04252-3.
- [11] K. Zheng, Y. Dong, J.H. Zheng, A. Foster, J. Lin, H. Dong, T.A. Dean, *Mater. Sci. Eng. A* **2019**, *761*, 138017. DOI: 10.1016/j.msea.2019.06.027.
- [12] B. Milkereit, M.J. Starink, P.A. Rometsch, C. Schick, O. Kessler, *Materials (Basel)* **2019**, *12*, 4083 DOI: 10.3390/MA12244083.
- [13] H. Mirzadeh, *Mater. Sci. Eng. A* **2021**, *819*, 141499. DOI: 10.1016/J.MSEA.2021.141499.
- [14] Z. Savaedi, H. Mirzadeh, R.M. Aghdam, R. Mahmudi, *J. Mater. Res. Technol.* **2022**, *19*, 3100. DOI: 10.1016/J.JMRT.2022.06.048.
- [15] X. Liu, L. Ye, J. Tang, B. Ke, Y. Dong, X. Chen, Y. Gu, *Mater. Sci. Eng. A.* **2022**, *848*, 143403. DOI: 10.1016/J.MSEA.2022.143403.
- [16] S.V. Sajadifar, A. Hosseinzadeh, J. Richter, M. Krochmal, T. Wegener, A. Bolender, A. Heidarzadeh, T. Niendorf, G.G. Yapici, *Adv. Eng. Mater.* **2022**, *24*, 2200384. DOI: 10.1002/ADEM.202200384.
- [17] S.V. Sajadifar, H.J. Maier, T. Niendorf, G.G. Yapici, *J. Eng. Mater. Technol.* **2020**, *142*, 1. DOI: 10.1115/1.4047747.
- [18] H. Li, X. Liu, Q. Sun, L. Ye, X. Zhang, *Mater.* **2020**, *13*, 2705. DOI: 10.3390/MA13122705.

- [19] A. Hosseinzadeh, A. Radi, J. Richter, T. Wegener, S.V. Sajadifar, T. Niendorf, G.G. Yapici, *J. Manuf. Process.* **2021**, *68*, 788. DOI: 10.1016/J.JMAPRO.2021.05.070.
- [20] B. Heider, E. Scharifi, T. Engler, M. Oechner, K. Steinhoff, *Materwiss. Werkstofftech.* **2021**, *52*, 145. DOI: 10.1002/MAWE.202000125.
- [21] M.K. Cavanaugh, R.G. Buchheit, N. Birbilis, *Eng. Fract. Mech.* **2009**, *76*, 641. DOI: 10.1016/J.ENGFRACMECH.2008.11.003.
- [22] F. Andreatta, H. Terryn, J.H.W. De Wit, *Electrochim. Acta* **2004**, *49*, 2851. DOI: 10.1016/J.ELECTACTA.2004.01.046.
- [23] N. Birbilis, M.K. Cavanaugh, R.G. Buchheit, *Corros. Sci.* **2006**, *48*, 4202. DOI: 10.1016/J.CORSCI.2006.02.007.
- [24] P.A. Rometsch, Y. Zhang, S. Knight, *Trans. Nonferrous Met. Soc. China* **2014**, *24*, 2003. DOI: 10.1016/S1003-6326(14)63306-9.
- [25] N.J.H. Holroyd, G.M. Scamans, *Metall. Mater. Trans. A* **2012**, *443*, 1230. DOI: 10.1007/S11661-012-1528-3.
- [26] B. Abeyrathna, B. Rolfe, M. Weiss, *Int. J. Adv. Manuf. Technol.* **2017**, *92*, 743. DOI: 10.1007/S00170-017-0164-X.
- [27] B. Milkereit, M. Österreich, P. Schuster, G. Kirov, E. Mukeli, O. Kessler, *Metals (Basel)*. **2018**, *8*, 531. DOI: 10.3390/met8070531.
- [28] E. Scharifi, S.V. Sajadifar, G. Moeini, U. Weidig, S. Böhm, T. Niendorf, K. Steinhoff, *Adv. Eng. Mater.* **2020**, *22*, 2000193. DOI: 10.1002/adem.202000193.
- [29] E. Scharifi, U. Savaci, Z.B. Kavaklioglu, U. Weidig, S. Turan, K. Steinhoff, *Mater. Charact.* **2021**, *174*, 111026. DOI: 10.1016/j.matchar.2021.111026.
- [30] E. Scharifi, R. Knoth, U. Weidig, *Procedia Manuf.* **2019**, *29*, 481. DOI: 10.1016/J.PROMFG.2019.02.165.
- [31] Y. Liu, B. Zhu, Y. Wang, S. Li, Y. Zhang, *Int. J. Light. Mater. Manuf.* **2020**, *3*, 20. DOI: 10.1016/J.IJLMM.2019.11.004.
- [32] D.K. Xu, P.A. Rometsch, N. Birbilis, *Mater. Sci. Eng. A* **2012**, *534*, 234. DOI: 10.1016/J.MSEA.2011.11.065.
- [33] H.-J. Christ, K. Lades, L. Völkl, H. Mughrabi, in *Low Cycle Fatigue and Elasto-Plastic Behaviour of Materials—3*, Springer Netherlands **1992**, DOI: 10.1007/978-94-011-2860-5_16.
- [34] A.H. Feng, D.L. Chen, Z.Y. Ma, *Metall. Mater. Trans. A*. **2010**, *41*, 957. DOI: 10.1007/s11661-009-0152-3.
- [35] P.V. Kumar, G.M. Reddy, K.S. Rao, *Def. Technol.* **2015**, *11*, 362. DOI: 10.1016/J.DT.2015.04.003.
- [36] H. Li, J. Liu, W. Yu, H. Zhao, D. Li, *Trans. Nonferrous Met. Soc. China* **2016**, *26*, 1191. DOI: 10.1016/S1003-6326(16)64250-4.
- [37] J.W. Evancho, J.T. Staley, *Metall. Mater. Trans. B* **1974**, *5*, 43. DOI: 10.1007/bf02642924.
- [38] J.T. Staley, *Mater. Sci. Technol.* **1987**, *3*, 923. DOI: 10.1179/mst.1987.3.11.923.
- [39] M.W. Mahoney, C.G. Rhodes, J.G. Flintoff, W.H. Bingel, R.A. Spurling, *Metall. Mater. Trans. A* **1998**, *29*, 1955. DOI: 10.1007/s11661-998-0021-5.
- [40] H. Aydın, A. Bayram, İ. Durgun, *Proc. Inst. Mech. Eng. Part C J. Mech. Eng. Sci.* **2013**, *227*, 649. DOI: 10.1177/0954406212452479.
- [41] C.G. Rhodes, M.W. Mahoney, W.H. Bingel, R.A. Spurling, C.C. Bampton, *Scr. Mater.* **1997**, *36*, 69. DOI: 10.1016/S1359-6462(96)-00344-2.
- [42] T.S. Srivatsan, D. Lanning, K.K. Soni, *J. Mater. Sci.* **1993**, *28*, 3205. DOI: 10.1007/BF00354237.
- [43] F. Schmid, P. Dumitraschkewitz, T. Kremmer, P.J. Uggowitzer, R. Tosone, S. Pogatscher, *Commun. Mater.* **2021**, *2*, 1. DOI: 10.1038/s43246-021-00164-9.
- [44] S. Hebbbar, L. Kertsch, A. Butz, *Metals (Basel)*. **2020**, *10*, 1. DOI: 10.3390/met10101361.
- [45] S.V. Sajadifar, E. Scharifi, T. Wegener, M. Krochmal, S. Lotz, K. Steinhoff, T. Niendorf, *Int. J. Fatigue* **2022**, *156*, 106676. DOI: 10.1016/J.IJFATIGUE.2021.106676.
- [46] M.J. Starink, *Mater. Sci. Eng. A*. **2005**, *390*, 260. DOI: 10.1016/J.MSEA.2004.09.053.
- [47] H.-J. Christ, H. Mughrabi, *Fatigue Fract. Eng. Mater. Struct.* **1996**, *19*, 335. DOI: 10.1111/j.1460-2695.1996.tb00971.

- [48] D.J. Lloyd, M.C. Chaturvedi, *J. Mater. Sci.* **1982**, 17, 1819. DOI: 10.1007/BF00540811.
- [49] A.S. El-Amoush, *Mater. Chem. Phys.* **2011**, 126, 607. DOI: 10.1016/J.MATCHEM-PHYS.2011.01.010.
- [50] A.P. Sekhar, A. Samaddar, A.B. Mandal, D. Das, *Met. Mater. Int.* **2020**, 27, 5059. DOI: 10.1007/S12540-020-00843-1.
- [51] W. Tian, S. Li, B. Wang, J. Liu, M. Yu, *Corros. Sci.* **2016**, 113, 1. DOI: 10.1016/J.CORSCI.2016.09.013.
- [52] N. Li, C. Dong, C. Man, X. Li, D. Kong, Y. Ji, M. Ao, J. Cao, L. Yue, X. Liu, M. Du, *Corros. Sci.* **2021**, 180, 109174. DOI: 10.1016/J.CORSCI.2020.109174.

Received in final form: August 8th 2022